Balance control using center of mass height variation: limitations imposed by unilateral contact

Twan Koolen,[1] Michael Posa,[1] and Russ Tedrake[1]

***Abstract*— Maintaining balance is fundamental to legged robots. The most commonly used mechanisms for balance control are taking a step, regulating the center of pressure ('ankle strategies'), and to a lesser extent, changing centroidal angular momentum (*e.g.*, 'hip strategies'). In this paper, we disregard these three mechanisms, instead focusing on a fourth: varying center of mass height. We study a 2D variable-height center of mass model, and analyze how center of mass height variation can be used to achieve balance, in the sense of convergence to a fixed point of the dynamics. In this analysis, we pay special attention to the constraint of unilateral contact forces. We first derive a necessary condition that must be satisfied to be able to achieve balance. We then present two control laws, and derive their regions of attraction in closed form. We show that one of the control laws achieves balance from any state satisfying the necessary condition for balance. Finally, we briefly discuss the relative importance of CoM height variation and other balance mechanisms.**

I. Introduction

Current methods for the analysis and control of balance for legged robots are often based on the dynamics of the robot's total linear and angular momentum. These 'centroidal dynamics' provide a useful low-dimensional projection of the full dynamics of the robot. Momentum-based control approaches [1], [2], [3], [4] can be used to translate strategies derived using the centroidal dynamics back to the full robot.

A key property of the centroidal dynamics is that only the wrenches acting *externally* on the robot can change its total momentum [5]. In fact, Euler's laws of motion state that the sum of external wrenches is equal to the rate of change of momentum. Despite these simple dynamics, the constraints on the external wrenches that can be exerted upon the robot are nontrivial: contact is unilateral, and forces must remain within friction cones.

Because of this, the centroidal dynamics are often further simplified by adding artificial constraints on the external wrenches, or equivalently, on the motion of the robot. Most commonly, angular momentum about the CoM is assumed to be constant (typically zero), and CoM height is assumed to be an affine (typically constant) function of horizontal CoM position. These assumptions define the Linear Inverted Pendulum (LIP) [6], which has long been a fixture in the design of balancing and walking controllers for legged robots. The LIP naturally leads to control strategies involving stepping and regulation of the center of pressure (CoP).

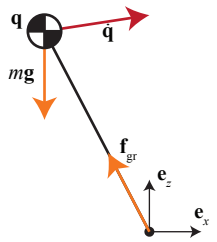

Fig. 1. Variable-height inverted pendulum model.

Although the LIP dynamics are easy to work with, the CoM height assumption in particular is overly constraining. This becomes apparent when the robot is *e.g.* required to dynamically step up onto a platform. Moreover, varying CoM height in an appropriate manner can be used as an additional mechanism to achieve balance.

Recently, efforts have been made to finally move away from the CoM height assumption. In [7], the dynamics of the divergent component of motion, also known as the instantaneous capture point, are extended to 3D and used to find a control law. In [8], numerical techniques are used to find quadratic height trajectories that solve the balancing problem for a variable-height inverted pendulum model. An important earlier work derived conditions that characterize when a given CoM height trajectory leads to balance [9], however without paying much attention to the constraint of unilateral contact.

This paper studies a 2D variable-height inverted pendulum model (see Fig. 1) and provides three main contributions. First, we derive an intuitively appealing outer approximation to the set of initial CoM positions and velocities that allow balance to be achieved, in the sense of convergence to a fixed point of the dynamics. Second, we design two *closed-form* balance control laws based on [9] (in contrast to the numerical techniques used in [8]). Third, we derive the exact regions of attraction of these control laws in closed form using quantifier elimination, explicitly taking unilateral contact into account. These regions of attraction are also inner approximations to the set of CoM states from which balance can be achieved. We show that the region of attraction for one of the controllers matches the outer approximation, and hence achieves balance from any state from which balance can possibly be achieved.

[1]All authors are with the Massachusetts Institute of Technology, 77 Massachusetts Avenue, Cambridge, MA 02139. {tkoolen, mposa, russt}@mit.edu

The remainder of the paper is structured as follows. Section II derives the dynamics of the variable-height model under consideration. Section III derives necessary conditions for balance, *i.e.*, the outer approximation. We then summarize the results of [9] (Section IV), which form the basis of the control laws (Section V) and the derivation of their regions of attraction (Section VI). We discuss our results in Section VII, and conclude the paper in Section VIII.

II. Variable-height inverted pendulum

The equations of motion of the 2D variable-height inverted pendulum (see Fig. 1) are

$$m\ddot{\mathbf{q}} = m\mathbf{g} + \mathbf{f}_{\text{gr}} \tag{1}$$

where $\mathbf{q} = (x, z)$ is the CoM position relative to the fixed point foot, m is robot's total mass, $\mathbf{g} = (0, -g)$ is the gravitational acceleration vector, and $\mathbf{f}_{\text{gr}}$ is the ground reaction force. We assume that angular momentum about the CoM remains constant, implying that the line of action of the ground reaction force must pass through the CoM. This allows the ground reaction force to be parameterized as

$$\mathbf{f}_{\text{gr}} = m\mathbf{q}u \tag{2}$$

where u is a scalar control input. Combining (2) and (1), we find

$$\ddot{\mathbf{q}} = \mathbf{g} + \mathbf{q}u \tag{3}$$

as the dynamics of the variable-height inverted pendulum. We assume unilateral contact (pulling on the ground is impossible), so we require that

$$u \geq 0. \tag{4}$$

By inspection, fixed points of the dynamics (3) must satisfy $\dot{x} = \dot{z} = 0$, $x = 0$, and $zu = g$, so $z > 0$. We are interested in achieving 'balance', in the sense of asymptotic convergence to a fixed point of the dynamics[1] at a specified desired final height $z = z_{\text{f}} > 0$.

Consider a state like the one depicted in Fig. 1, and suppose the initial horizontal velocity, $\dot{x}$, is 'too large' in some sense. To achieve balance, a large value of u can be used to decrease $\dot{x}$ quickly. However, this also has the effect of increasing $\dot{z}$, and over time, z, as a byproduct. The challenge is to control both horizontal and vertical CoM position with a single control input by exploiting the state-dependent variation of the effect of u in the nonlinear dynamics (3).

III. Necessary conditions for balance

In this section we investigate conditions that must be satisfied in any case if balance is to be achieved.

Let the state of the variable-height inverted pendulum be $\mathbf{x} = (x, z, \dot{x}, \dot{z})$. Starting from $\mathbf{x}$, convergence to the fixed point requires that the horizontal CoM position x and velocity $\dot{x}$ satisfy

$$x\dot{x} < 0 \tag{5}$$

This is because $\dot{x}$ would otherwise increase without bound, since (3) and (4) imply that $\text{sign}(\ddot{x}) = \text{sign}(x)$.

Another necessary condition for balance stems from the extreme control policy of choosing $u = 0$ for all time. This policy results in a ballistic CoM trajectory. We will show that it is impossible to reach a fixed point of the dynamics from state $\mathbf{x}$ if the z-intercept of the ballistic trajectory starting from $\mathbf{x}$ is nonpositive, making it impossible to achieve balance.

The ballistic trajectory starting from state $\mathbf{x}$ is

$$\mathbf{q}_{\text{bal}}(\mathbf{x}, t) = \begin{bmatrix} x_{\text{bal}}(\mathbf{x}, t) \\ z_{\text{bal}}(\mathbf{x}, t) \end{bmatrix} = \begin{bmatrix} x + \dot{x}t \\ z + \dot{z}t - \frac{1}{2}gt^2 \end{bmatrix}. \tag{6}$$

Let T be the time at which $x_{\text{bal}}(\mathbf{x}, T) = 0$, $T = -\frac{x}{\dot{x}}$, and let

$$z_{\text{crit}}(\mathbf{x}) = z_{\text{bal}}(\mathbf{x}, T) = z - \frac{\dot{z}x}{\dot{x}} - \frac{gx^2}{2\dot{x}^2}$$

be the z-intercept of the ballistic trajectory.

Lemma 1: Suppose $z_{\text{crit}}(\mathbf{x}) \leq 0$ and assume (5), so that $T \geq 0$. Then no state $\mathbf{x}_{\text{f}} = (x_{\text{f}}, z_{\text{f}}, \dot{x}_{\text{f}}, \dot{z}_{\text{f}})$ for which $x_{\text{f}} = 0$ and $z_{\text{f}} > 0$ is reachable from $\mathbf{x}$ given the dynamics (3) and input limit (4).

Proof: The time derivative of $z_{\text{crit}}(\mathbf{x})$ along trajectories of (3) is

$$\begin{aligned} \frac{d}{dt} z_{\text{crit}}(\mathbf{x}) &= \frac{\partial z_{\text{crit}}(\mathbf{x})}{\partial \mathbf{q}}\dot{\mathbf{q}} + \frac{\partial z_{\text{crit}}(\mathbf{x})}{\partial \dot{\mathbf{q}}}(\mathbf{g} + \mathbf{q}u) \\ &= u\frac{x}{\dot{x}}\frac{1}{\dot{x}^2}\left(gx^2 + \dot{x}(x\dot{z} - \dot{x}z)\right). \end{aligned}$$

The condition $z_{\text{crit}}(\mathbf{x}) \leq 0$ can be rearranged to find

$$\dot{x}(x\dot{z} - \dot{x}z) \geq -\frac{gx^2}{2}.$$

Together with $u \geq 0$ according to (3), $\frac{x}{\dot{x}} < 0$ according to (5), and $g > 0$, we infer that

$$\frac{d}{dt} z_{\text{crit}}(\mathbf{x}) \leq 0$$

so we conclude that z_{crit} cannot increase along trajectories of (3), and if $z_{\text{crit}}(\mathbf{x}_{\text{f}}) > z_{\text{crit}}(\mathbf{x})$, then $\mathbf{x}_{\text{f}}$ must not be reachable from $\mathbf{x}$. Noting that $z_{\text{crit}}(\mathbf{x}_{\text{f}}) = z_{\text{f}}$ and $z_{\text{f}} > z_{\text{crit}}(\mathbf{x})$ completes the proof. ∎

Since any fixed point of the dynamics must satisfy $x_{\text{f}} = 0$ and $z_{\text{f}} > 0$, Lemma 1 provides the condition

$$z_{\text{crit}}(\mathbf{x}) > 0 \tag{7}$$

as a useful outer approximation of the set of states that allow balance. In the following sections, we will derive a feedback control law with a region of attraction described exactly by (7), assuming only unilateral contact and no kinematic constraints or actuation limits. This will show that the outer approximation is tight.

[1] Note that we are not interested in achieving asymptotic *stability* of a fixed point, which is impossible in the variable-height inverted pendulum.

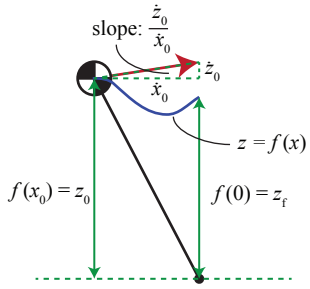

Fig. 2. Kinematic constraints placed on CoM height trajectory f.

IV. Approach and summary of previous results

Our general approach to control is to design and enforce a virtual constraint [10]. Virtual constraints were first applied to the variable-height inverted pendulum in [9]. This section summarizes their results, providing no new contributions.

A. Height trajectory as a virtual constraint

Consider the time-invariant virtual holonomic constraint

$$z = f(x) \tag{8}$$

where f describes a desired CoM height trajectory.

We will assume that the initial value and slope of the CoM height trajectory match the initial state $\mathbf{x}_0 = (x_0, z_0, \dot{x}_0, \dot{z}_0)$, as depicted in Fig. 2:

$$f(x_0) = z_0 \tag{9a}$$

$$f'(x_0) = \frac{\dot{z}_0}{\dot{x}_0}. \tag{9b}$$

Differentiating (8) twice with respect to time gives

$$\ddot{z} = f'(x)\,\ddot{x} + f''(x)\,\dot{x}^2.$$

Substituting this into (3), we can solve for the input u required to enforce the virtual constraint:

$$u = \frac{g + f''(x)\,\dot{x}^2}{\bar{f}(x)} \tag{10}$$

where

$$\bar{f}(x) = f(x) - f'(x)\,x. \tag{11}$$

The dynamics of the unconstrained degree of freedom x are simply

$$\ddot{x} = ux. \tag{12}$$

Example 1: For the LIP, f is an affine function, fully specified by the continuity constraints (9):

$$f(x) = z_0 + \frac{\dot{z}_0}{\dot{x}_0}x.$$

The required input simplifies to a constant,

$$u = \frac{g}{z_0}$$

showing that as long as $z_0 > 0$, the condition $u \geq 0$ is always satisfied (no pulling on the ground). Equation (12) becomes

$$\ddot{x} = \frac{g}{z_0}x, \tag{13}$$

the familiar LIP dynamics. ▲

By not artificially constraining f to be an affine function, balance can be achieved from more initial states than what is allowed by the LIP dynamics. We now investigate how the requirement of achieving balance constrains f.

B. Orbital energy

Orbital energy can be used to decide which states converge to the fixed point while tracking a given height trajectory f.[2] We will first introduce orbital energy for the LIP, and then generalize to arbitrary f.

1) LIP: For the LIP, orbital energy [6] is a well-known conserved quantity, defined as:

$$E_{\text{LIP}}(x, \dot{x}) = \frac{1}{2}\dot{x}^2 - \frac{g}{2z_0}x^2. \tag{14}$$

The fact that LIP orbital energy is conserved can be shown by taking the time derivative of (14) and plugging in the dynamics (13). To achieve balance, conservation of orbital energy implies that the initial orbital energy must be the same as the orbital energy at the fixed point,

$$E_{\text{LIP}}(x_0, \dot{x}_0) = E_{\text{LIP}}(0, 0) = 0$$

If (5) is also satisfied at $\mathbf{x}_0$, this results in the familiar condition

$$x_0 + \sqrt{\frac{z_0}{g}}\dot{x}_0 = 0. \tag{15}$$

The left hand side is known as the instantaneous capture point [11], [12], extrapolated center of mass [13], or divergent component of motion [14].

2) Variable-height model: Perhaps a less known fact is that a conserved orbital energy exists for *any* C^2 height trajectory f. As derived in [9], the orbital energy associated with f is

$$E_f(x, \dot{x}) = \frac{1}{2}\dot{x}^2\bar{f}^2(x) + gx^2 f(x) - 3g\int_0^x f(\xi)\,\xi d\xi \tag{16}$$

with $\bar{f}(x)$ as defined in (11). Analogous to the LIP, the fact that orbital energy is conserved can be (tediously) verified by taking the time derivative and plugging in the dynamics (12). Again, balance requires that x_0 and $\dot{x}_0$ have opposite sign and that

$$E_f(x_0, \dot{x}_0) = E_f(0, 0) = 0.$$

With the continuity constraints from (9), this requirement simplifies to

$$3g\int_0^{x_0} f(\xi)\,\xi d\xi = k \tag{17}$$

[2]Note that orbital energy is *not* the same as the total energy of the system.

with

$$k = \frac{1}{2}\left(\dot{x}_0 z_0 - \dot{z}_0 x_0\right)^2 + g x_0^2 z_0.$$

In general, the integral on the left hand side of (17) may not be computable in closed form, but if we restrict the class of height trajectories f to polynomials,

$$f(x) = \sum_{i=0}^{n} c_i x^i,$$

then the integral is readily evaluated and (17) can be written as a linear constraint on the coefficients c_i:

$$3g \sum_{i=0}^{n} \frac{1}{i+2} c_i x_0^{i+2} = k. \tag{18}$$

This constraint will be used to find a feedback control law in the following section.

V. Control laws

This section presents two feedback control laws based on virtual constraints and orbital energy.

We will take height trajectory f to be a cubic polynomial ($n = 3$), and impose four linear constraints that uniquely determine its coefficients:

1) the final desired height: $f(0) = z_\mathrm{f}$;
2–3) the continuity constraints (9);
4) the orbital energy constraint (18).

These constraints can be written concisely as

$$\underbrace{\begin{bmatrix} 1 & 0 & 0 & 0 \\ 1 & x_0 & x_0^2 & x_0^3 \\ 0 & 1 & 2x_0 & 3x_0^2 \\ \frac{3}{2}gx_0^2 & gx_0^3 & \frac{3}{4}gx_0^4 & \frac{3}{5}gx_0^5 \end{bmatrix}}_{\mathbf{A}} \begin{bmatrix} c_0 \\ c_1 \\ c_2 \\ c_3 \end{bmatrix} = \begin{bmatrix} z_\mathrm{f} \\ z_0 \\ \frac{\dot{z}_0}{\dot{x}_0} \\ k \end{bmatrix}.$$

The determinant of matrix $\mathbf{A}$ is $\frac{g x_0^7}{10}$, showing that a solution exists as long as $x_0 \neq 0$.

We omit the solution for the coefficients c_i here, since the expressions are somewhat long and uninformative. It is important to note however that the c_i will depend *rationally* on $\mathbf{x}_0$ (as well as z_f and g). Substituting the c_i back into f shows that f is also a rational function of x and $\mathbf{x}_0$. We can even find u in closed form,[3] as a rational function of x and $\mathbf{x}_0$ after substitution into (10):

$$u = U(x, \mathbf{x}_0) = \frac{p(x, \mathbf{x}_0)}{q(x, \mathbf{x}_0)} \tag{19}$$

where $p(x, \mathbf{x}_0)$ and $q(x, \mathbf{x}_0)$ are polynomials of respective total degrees 20 and 21 in the variables $(x, \mathbf{x}_0)$.

To arrive at a feedback controller, our strategy is to essentially 'continually re-solve' for the CoM height trajectory f by substituting the current state $\mathbf{x}$ for $\mathbf{x}_0$ in (19), a form of explicit model predictive control. This substitution also greatly simplifies the expression. The resulting control law is:

$$u = U(x, \mathbf{x}) = -7a^2 + \frac{3 z_\mathrm{f} a^3 - g a}{b} - \frac{10 a^3 b}{g}. \tag{20}$$

[3]Note that the term $\dot{x}^2$ in (10) can be solved for given f and x using (16), since $E_f(x, \dot{x}) = 0$ by construction of f.

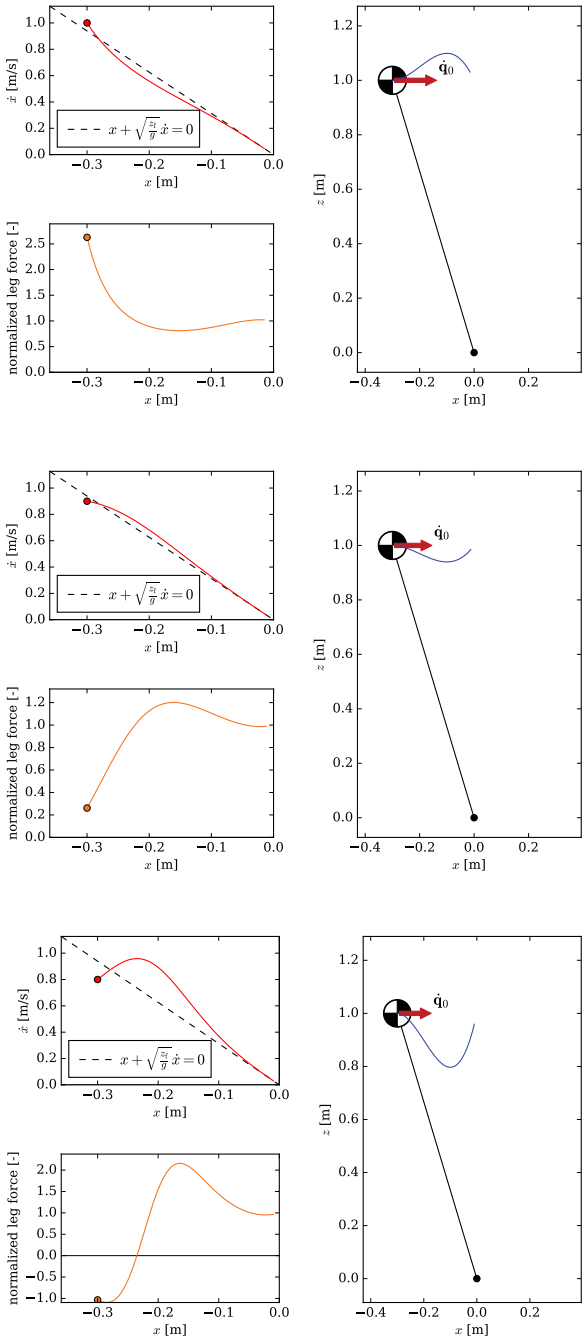

Fig. 3. Simulation results for orbital energy controller (20) with initial conditions $x_0 = -0.3$ [m], $z_0 = 1$ [m], $\dot{z}_0 = 0$ [m/s] and three values of $\dot{x}_0$: 1.0 [m/s] (top), 0.9 [m/s] (middle), and 0.8 [m/s] (bottom). The normalized leg force is computed as $\frac{\mathbf{f}_\mathrm{gr}}{mg} \cdot \frac{\mathbf{q}}{\|\mathbf{q}\|} \equiv \frac{1}{g} u \|\mathbf{q}\|$. For this plot, $g = 9.8$ [m/s^2], $z_\mathrm{f} = 1$ [m]. For the third (slowest) initial condition, the simulation was performed as if pulling on the ground were possible.

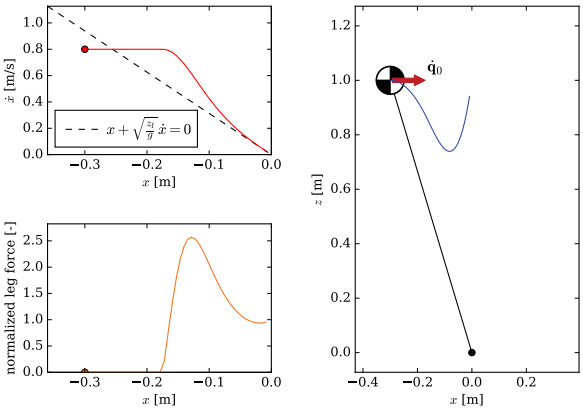

Fig. 4. Simulation results for clipped controller (22) with initial conditions $x_0 = -0.3$ [m], $z_0 = 1$ [m], $\dot{x}_0 = 0.8$ [m/s], and $\dot{z}_0 = 0$ [m/s]. For this plot, $g = 9.8$ [m/s^2], $z_\mathrm{f} = 1$ [m].

with

$$a = \frac{\dot{x}}{x} \qquad\qquad b = \dot{z} - az. \tag{21}$$

We will refer to this control law as the 'orbital energy controller'. The orbital energy controller has the property that it keeps the CoM height on the cubic height trajectory f in the absence of external disturbances to the dynamics (3). This is because the control law ensures that $\dot{\mathbf{x}}$ is tangent to the constraint manifold described by $z = f(x)$ since it stems from (10), and because f is uniquely specified by the initial conditions.

Note the singularities at $x = 0$ and $b = 0$. The singularity at $x = 0$ is due to the fundamental lack of effect of the control input u on $\ddot{x}$ when $x = 0$. The singularity at $b = 0$ occurs when the CoM velocity vector points from the CoM toward the point foot. This implies that the necessary condition for balance derived earlier, (7), is not satisfied, so states for which $b = 0$ are not of interest. The root cause of this singularity is the fact that the input u that enforces constraint (8) is not uniquely defined in this case.

See Fig. 3 for the results of simulations with the orbital energy controller, starting from three example initial conditions. Note that the orbital energy controller will attempt to pull on the ground if the initial velocity is very low, as shown by the negative normalized ground reaction forces. To address this, we will also consider the following 'clipped controller':

$$u = \max\left(U\left(x, \mathbf{x}\right), 0\right). \tag{22}$$

Fig. 4 shows that the clipped controller (22) successfully achieves balance at the same initial velocity that resulted in pulling on the ground with orbital energy controller (20).

In addition to the limitation of unilateral contact, there are two other issues that require more attention compared to the LIP:

1) the CoM height trajectory may not be kinematically feasible due to robot geometry and joint limits;
2) actuation limits may be violated.

Barring unilaterality of contact, kinematics, and actuations limits, it would be possible to achieve balance from any state. In this paper, we choose not to address kinematics or actuation limits, as they are robot specific. Instead, we focus on the fundamental implications of unilateral contact.

VI. Region of attraction

We now derive the regions of attraction of the orbital energy controller (20) (in Section VI-A) and the clipped controller (22) (in Section VI-B). These regions of attraction are also inner approximations of the set of initial states from which balance can be achieved. The inner approximation for the clipped control law will turn out to be the same as the outer approximation derived in Section III.

A. Orbital energy controller

For the orbital energy controller (20), observe that if (5) holds, then by construction of f, x will converge to 0, so x is between x_0 and 0 for all time. Hence, requiring that $u \geq 0$ for all time is the same as requiring (5) and

$$U\left(\delta x_0, \mathbf{x}_0\right) \geq 0 \quad \forall \delta \in [0, 1] \tag{23}$$

The task is now to find an explicit description of the set of initial conditions that satisfy (23). Condition (23) can be written equivalently as

$$p\left(\delta x_0, \mathbf{x}_0\right) q\left(\delta x_0, \mathbf{x}_0\right) \geq 0 \quad \forall \delta \in [0, 1]\,. \tag{24}$$

The conditions (5) and (24) together form a *first-order formula* over the reals in the variables $\mathbf{x}_0, \delta, g, z_\mathrm{f}$ [15]. For completeness, we should add that $g > 0$ and $z_\mathrm{f} > 0$.

In this context, a first-order formula in variables $y_1, \ldots, y_n$ is an expression written by combining a set of polynomial equations and inequalities in $y_1, \ldots, y_n$ using the logical conjunction ($\wedge$), disjunction ($\vee$), and negation ($\neg$) operators, while some or all of the variables are quantified over by universal and/or existential quantifiers (*e.g.*, $\forall y_1$, $\exists y_2$). Variables that are not quantified over are called free. For any first-order formula over the reals, there is an equivalent *quantifier-free* formula, *i.e.*, a formula without any universal or existential quantifiers, by the famous Tarski-Seidenberg theorem [16]. The process of finding an equivalent quantifier-free formula is known as quantifier elimination.

Example 2: [15] Quantifier elimination can be applied to the first-order formula

$$a \neq 0 \wedge \left(\exists x \text{ such that } ax^2 + bx + c = 0\right)$$

in variables a, b, c, x (with a, b, c free) to find the familiar equivalent quantifier-free formula $b^2 - 4ac \geq 0$. ▲

Cylindrical Algebraic Decomposition (CAD) methods can be used to solve quantifier elimination problems

[15]. The worst case running time of modern CAD-based algorithms is polynomial in the number of polynomials in the input formula and their degree, but exponential in the number of free variables [15]. Implementations include QEPCAD B [17] and Mathematica's `CylindricalDecomposition` function [18].

We used Mathematica's implementation to find a quantifier-free formula that is equivalent to the conjunction of (24), (5), $g > 0$ and $z_\mathrm{f} > 0$. It should be noted that applying the CAD algorithm directly took too long, but using the variable substitutions

$$a_0 = \frac{\dot{x}_0}{x_0} \qquad\qquad b_0 = \dot{z}_0 - a_0 z_0$$

analogous to (21), we were able to reduce the number of free variables in (23) from six ($\mathbf{x}_0$, g, and z_f) to four (a_0, b_0, g, and z_f), which made the problem tractable. After conversion to a first-order formula (analogous to the step from (23) to (24)), the CAD algorithm was able to solve the problem in less than two seconds. The result (after simplification) is that initial states must satisfy

$$a_0 < 0 \wedge 7g + 20a_0 b_0 + \sqrt{9g^2 + 120a_0^2 g z_\mathrm{f}} \leq 0. \qquad (25)$$

See Fig. 5 for a 3D slice of this region at $\dot{z}_0 = 0$, in terms of x_0, $\dot{x}_0$, and z_0. See Fig. 6 for a 2D slice at $\dot{z}_0 = 0$ and $z_0 = z_\mathrm{f}$, as well as a comparison to the region for the LIP with fixed point foot, a line defined by the instantaneous capture point, and the necessary condition (7).

For $\dot{z}_0 = 0$ and fixed z_0, Figs. 5 and 6 show that balance can be achieved from a double cone in the $(x_0, \dot{x}_0)$ plane, with a nappe in each quadrant where x_0 and $\dot{x}_0$ have opposite sign. The double cone geometry is due to the fact that in (25), x_0 and $\dot{x}_0$ only appear as the ratio $a_0 = \frac{\dot{x}_0}{x_0}$. Informally speaking, the 'size' of the double cone increases as z_0 increases, as can be expected from intuition. Increasing $\dot{z}_0$ also grows the double cone (not shown in figures). If $\dot{z}_0 > 0$, there exist (unrealistic) states with $z_0 < 0$ for which balance can be achieved.

Figs. 5 and 6 suggest (for $\dot{z} = 0$) that if balance can be achieved from $(x_0, z_0, \dot{x}_0, \dot{z}_0)$, then balance can also be achieved from $(x_0, z_0, c\dot{x}_0, \dot{z}_0)$, for any $c \geq 1$. In other words, dilating the initial horizontal velocity can never compromise the ability to achieve balance. Indeed, we were able to prove this dilation property for any $\dot{z}_0$ using Mathematica functions, including the same CAD techniques described earlier, as long as $z_0 > 0$.[4] This implies that for fixed x_0, $\dot{z}_0$, and $z_0 > 0$, the constraint $u \geq 0$ and the restriction to cubic CoM height trajectories only impose a *lower* limit on the initial velocity at which the CoM approaches $x = 0$, and no upper limit. An upper limit could come from the robot's kinematics or actuation limits, which were not investigated in this paper. Indeed, for high initial velocities, the CoM trajectory can reach unrealistically high values.

[4]For the unrealistic case of $z_0 \leq 0$, a counterexample was found with $a_0 = -1$, $z_0 = -\frac{9}{16}$, $\dot{z}_0 = \frac{13}{8}$, $c = 2$, $g = 1$, and $z_\mathrm{f} = 1$.

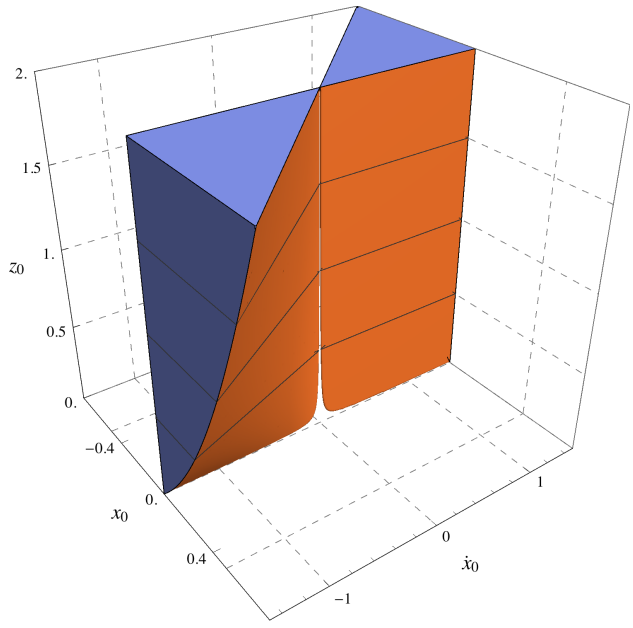

Fig. 5. Slice at $\dot{z}_0 = 0$ of the set of states from which balance can be achieved. It is important to note that the apparent separation between the regions on opposite sides of the $\dot{x}_0$-axis is merely a plotting artifact. For this plot, $g = 9.8$ [m/s^2], $z_\mathrm{f} = 1$ [m]. The full region extends outside the borders of the plot, to infinity, along the blue sections.

The double cone in Fig. 6 can be compared to the line defined by the instantaneous capture point for the LIP, (15). The most interesting comparison is between the LIP line and the line associated with the lower limit on horizontal velocity for the variable-height model, for the case $z_0 = z_\mathrm{f}$. The slope of this line can be found by maximizing a_0 subject to (25). For $z_0 = z_\mathrm{f}$ and $\dot{z}_0 = 0$, the optimal value can be found in closed form, and we have

$$a_0 = \frac{\dot{x}_0}{x_0} \leq -\sqrt{\frac{5+\sqrt{15}}{10}}\sqrt{\frac{g}{z_0}} \approx -0.94\sqrt{\frac{g}{z_0}}. \qquad (26)$$

We can compare this to the LIP by rewriting (15) as

$$\frac{\dot{x}_0}{x_0} = -\sqrt{\frac{g}{z_0}}$$

which shows that for a given value of x_0, the presented approach can achieve balance from states that have an initial horizontal velocity up to ~6% slower compared to the LIP.

We can also compare this lower velocity limit to the necessary condition derived from the ballistic trajectory in Section III. With $\dot{z}_0 = 0$, condition (7) evaluated at $\mathbf{x} = \mathbf{x}_0$ can be rearranged to find

$$\frac{\dot{x}_0}{x_0} < -\frac{1}{\sqrt{2}}\sqrt{\frac{g}{z_0}} \approx -0.71\sqrt{\frac{g}{z_0}} \qquad (27)$$

implying that for fixed x_0, it is *impossible* to achieve balance from initial horizontal velocities that are more than ~39% lower than the balancing velocity for the LIP.

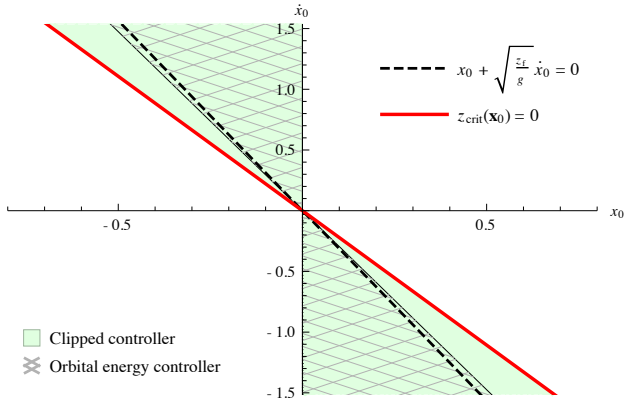

Fig. 6. Set of states from which balance can be achieved; comparison between LIP (region defined by (15), the instantaneous capture point), orbital energy controller (region defined by (25)), and clipped controller (which corresponds to the necessary condition for balance $z_{\text{crit}}(\mathbf{x}) > 0$). Slice at $\dot{z}_0 = 0$ and $z_0 = z_f$ for the variable-height inverted pendulum. For this plot, $g = 9.8$ [m/s^2], $z_f = 1$ [m].

B. Clipped controller

We now use the results for the orbital energy controller to derive the region of attraction of the clipped controller.

Note that if the orbital energy controller produces $u < 0$, then the output of the clipped controller, (22), is $u = 0$, meaning that the CoM will follow the ballistic trajectory (6). We will show that for any state satisfying necessary condition (7), following the ballistic trajectory will eventually bring the state in the region of attraction (25) of the orbital energy controller.

For states satisfying (5), following the ballistic trajectory means that $\dot{x}$ remains constant and $|x|$ decreases. This implies that the ratio $a = \frac{\dot{x}}{x}$ will approach $-\infty$ as x approaches 0. We will therefore examine what happens to the functions describing the region of attraction of the orbital energy controller as a_0 approaches $-\infty$. The first condition in (25), $a_0 < 0$, will certainly be satisfied. The second condition in (25) will also be satisfied, as long as $z_0 > 0$:

$$\lim_{a_0 \to -\infty} 7g + 20a_0\dot{z}_0 - 20a_0^2 z_0 + \sqrt{9g^2 + 120a_0^2 g z_f} = -\infty z_0 \leq 0$$

since the quadratic term dominates. Here, we have substituted the definition $b_0 = \dot{z}_0 - a_0 z_0$ into (25).

We now note that if necessary condition (7) is satisfied, then following the ballistic trajectory will make $z > 0$ in some open interval around $x = 0$, so $z_0 > 0$ will indeed be satisfied as $a_0 \to -\infty$. We thus conclude that the region of attraction of (22) matches the outer approximation given by (7): if the ballistic trajectory starting from the current state has a z-intercept greater than zero, then the clipped controller (22) will make the state converge to the fixed point at $z = z_f$.

VII. Discussion

A limitation of the presented control approach is that, similar to typical LIP-based approaches, kinematic limits and actuator limits are not taken into account. This poses more of a problem for the presented variable-height model than for the LIP. Indeed, using control laws (20) or (22), ground reaction forces and CoM heights may become very large for high initial horizontal velocities, *i.e.* with a large value of $-\frac{\dot{x}_0}{x_0}$. For the clipped controller, similar issues occur at very low initial horizontal velocities. Very slow initial conditions result in entering the region of attraction of the orbital energy controller at a very large value of $-\frac{\dot{x}_0}{x_0}$, resulting in extreme control actions. More work is needed to study the constraints that kinematics and actuation limits impose on the ability to achieve balance using CoM height control.

The presented model and approach do not explicitly take friction cone constraints into account. However, the angle between the ground reaction force vector $\mathbf{f}_{\text{gr}}$ and the vertical axis is the same as the angle between the CoM position, $\mathbf{q}$, and the vertical axis. It can be shown that if balance is achievable from initial state $\mathbf{x}_0$ according to (25) then the greatest angle between $\mathbf{q}$ and the vertical axis that occurs while using either controller presented in this paper is at $\mathbf{x}_0$.

With these caveats in mind, the analysis presented in this paper can still provide insight into the relative importance of CoM height control and other balancing mechanisms. Since the clipped orbital energy controller (22) achieves balance from any state that satisfies necessary condition (7), (27) applies: the controller achieves balance from initial horizontal CoM velocities that are up to 39% lower than the horizontal velocity that results in balance for the LIP, a significant difference. In the presence of kinematic constraints and actuation limits, this provides a useful upper bound on the effectiveness of CoM height control. The limit of 6% given by (26), corresponding to tracking a cubic CoM height trajectory with the unclipped orbital energy controller, perhaps provides a more realistic assessment when kinematic constraints and actuation limits are present. An interesting property of CoM height control is that its effectiveness, quantified in terms of a lower limit on horizontal CoM velocity, increases with horizontal displacement between the CoM and the point foot, as shown by (27). This is in contrast to stepping, CoP control, and control of centroidal angular momentum, for which effectiveness does not depend on horizontal CoM position at a fixed horizontal CoM velocity [12]. For $x_0 = -0.4$ [m], $z_0 = z_f = 1$ [m], $g = 9.8$ [m/s^2], and $\dot{z}_0 = 0$ [m/s], CoM height control can be used to achieve balance from the same lower limit on $\dot{x}_0$ as could be achieved with a 2.3 [cm] change in CoP for the orbital energy controller, and an 11.7 [cm] change for the clipped controller (executing a ballistic trajectory).

Assessing to what degree CoM height control is used

for balance in humans is an interesting topic. Long jump athletes that land on their feet can be observed to keep their CoM height low during the landing phase to avoid falling backwards, which would decrease their distance. Humans seem to increase their CoM height when required to stop abruptly without taking additional steps. It would be interesting to know to what degree humans vary CoM height (with respect to a nominal trajectory) in order to regain balance during more periodic motions, such as walking and running.

We note that extending our results to a 3D model is not trivial, contrary to the LIP. Typically, virtual constraint approaches shine when the degree of underactuation[5] is one. A possible direction of future research is to include *e.g.* lateral center of pressure control as an additional input in a 3D model, so as to maintain one degree of underactuation. Another possible approach is to use decoupled lateral and sagittal plane controllers [19]. In general, combining CoM height control with the use of other stabilizing mechanisms is a topic of future research.

In this paper, we employed quantifier elimination techniques. While these techniques can be extremely powerful, they do not scale well. In addition, the end results are not always as clean as condition (25). Nevertheless, there may be other problems in legged locomotion that could benefit from the application of these techniques.

VIII. Conclusion

This paper investigated the use of center of mass height variation to achieve balance, subject to the constraint of unilateral contact. For a 2D variable-height inverted pendulum model, we derived an outer approximation of the set of states from which balance is achievable. We presented a controller for the variable-height inverted pendulum based on orbital energy, and derived its region of attraction. We also studied a clipped version of the orbital energy controller, and showed that it achieves balance from any state for which it is physically possible to achieve balance.

References

[1] S. Kajita, F. Kanehiro, K. Kaneko, K. Fujiwara, K. Harada, K. Yokoi, and H. Hirukawa, "Resolved momentum control: humanoid motion planning based on the linear and angular momentum," in *Proc. 2003 IEEE/RSJ Int. Conf. Intelligent Robots and Systems*, vol. 2. IEEE, 2003, pp. 1644–1650.

[2] S.-H. Lee and A. Goswami, "A Momentum-based Balance Controller for Humanoid Robots on Non-level and Non- stationary Ground," *Autonomous Robots*, vol. 33, no. 4, pp. 399–414, 2012.

[3] A. Herzog, N. Rotella, S. Mason, F. Grimminger, S. Schaal, and L. Righetti, "Momentum control with hierarchical inverse dynamics on a torque-controlled humanoid," *Autonomous Robots*, vol. 40, no. 3, pp. 473–491, 2016.

[4] T. Koolen, S. Bertrand, G. Thomas, T. De Boer, T. Wu, J. Smith, J. Englsberger, and J. Pratt, "Design of a momentum-based control framework and application to the humanoid robot atlas," *International Journal of Humanoid Robotics*, vol. 13, no. 01, p. 1650007, 2016.

[5]Roughly speaking, the number of degrees of freedom minus the number of inputs.

[5] D. E. Orin, A. Goswami, and S.-H. Lee, "Centroidal dynamics of a humanoid robot," *Autonomous Robots*, no. September 2012, pp. 1–16, Jun. 2013.

[6] S. Kajita and K. Tani, "Study of dynamic biped locomotion on rugged terrain-derivation and application of the linear inverted pendulum mode," in *Robotics and Automation, 1991. Proceedings., 1991 IEEE International Conference on*, Apr 1991, pp. 1405–1411 vol.2.

[7] J. Englsberger, C. Ott, and A. Albu-Schäffer, "Three-dimensional bipedal walking control using divergent component of motion," in *Intelligent Robots and Systems (IROS), 2013 IEEE/RSJ International Conference on*, Nov 2013, pp. 2600–2607.

[8] O. E. Ramos and K. Hauser, "Generalizations of the capture point to nonlinear center of mass paths and uneven terrain," in *Humanoid Robots (Humanoids), 2015 IEEE-RAS 15th International Conference on*, Nov 2015, pp. 851–858.

[9] J. E. Pratt and S. V. Drakunov, "Derivation and application of a conserved orbital energy for the inverted pendulum bipedal walking model," in *Robotics and Automation, 2007 IEEE International Conference on*, April 2007, pp. 4653–4660.

[10] A. Shiriaev, J. W. Perram, and C. Canudas-de Wit, "Constructive tool for orbital stabilization of underactuated nonlinear systems: Virtual constraints approach," *Automatic Control, IEEE Transactions on*, vol. 50, no. 8, pp. 1164–1176, 2005.

[11] J. Pratt, J. Carff, S. Drakunov, and A. Goswami, "Capture point: A step toward humanoid push recovery," in *Humanoid Robots, 2006 6th IEEE-RAS International Conference on*, Dec 2006, pp. 200–207.

[12] T. Koolen, T. De Boer, J. Rebula, A. Goswami, and J. Pratt, "Capturability-based analysis and control of legged locomotion, part 1: Theory and application to three simple gait models," *The International Journal of Robotics Research*, vol. 31, no. 9, pp. 1094–1113, 2012.

[13] A. L. Hof, M. Gazendam, and W. Sinke, "The condition for dynamic stability," *Journal of Biomechanics*, vol. 38, no. 1, pp. 1–8, 2005.

[14] T. Takenaka, T. Matsumoto, and T. Yoshiike, "Real time motion generation and control for biped robot-1 st report: Walking gait pattern generation," in *2009 IEEE/RSJ International Conference on Intelligent Robots and Systems*. IEEE, 2009, pp. 1084–1091.

[15] B. F. Caviness and J. R. Johnson, *Quantifier elimination and cylindrical algebraic decomposition*. Springer Science & Business Media, 2012.

[16] A. Seidenberg, "A new decision method for elementary algebra," *Annals of Mathematics*, pp. 365–374, 1954.

[17] C. W. Brown, "QEPCAD B: a program for computing with semi-algebraic sets using CADs," *ACM SIGSAM Bulletin*, vol. 37, no. 4, pp. 97–108, 2003.

[18] A. Strzeboński, "Solving systems of strict polynomial inequalities," *Journal of Symbolic Computation*, vol. 29, no. 3, pp. 471–480, 2000.

[19] X. Da, O. Harib, R. Hartley, B. Griffin, and J. W. Grizzle, "From 2D design of underactuated bipedal gaits to 3D implementation: Walking with speed tracking," *IEEE Access*, vol. 4, pp. 3469–3478, 2016.